FEBS Letters 450 (1999) 144–148 FEBS 21896

Modelling charge interactions in the prion protein: predictions for pathogenesis

James Warwicker[1,*]

Institute of Food Research, Reading Laboratory, Whiteknights Road, Reading RG6 6BZ, UK

Received 4 February 1999; received in revised form 18 March 1999

Abstract Calculations are presented for the pH-dependence of stability and membrane charge complementarity of prion protein fragments. The theoretical results are compared with reported characterisations of prion protein folding in vitro. Discussion of models for conformational change and pathogenesis in vivo leads to the prediction of amino acids that could mediate sensitivity to the endosomal pH and to a design strategy for recombinant prion proteins with an increased susceptibility to prion protein^{Sc}-like properties in vitro. In this model, the protective effect of certain basic polymorphisms can be interpreted in terms of oligomerisation on a negatively-charged surface.

Key words: Prion protein; pH-dependence; Molecular modelling; Protein electrostatic; Transmissible spongiform encephalopathy

1. Introduction

Whilst the precise nature of the infectious agent in transmissible spongiform encephalopathies (TSEs) remains unknown [1], a large amount of data implicate the protease resistant form of PrP [2], denoted PrP^{Sc} in contrast to the cellular protease-sensitive form, PrP^{C}. Models to account for pathogenesis within a protein-only framework have focussed on conformational differences between PrP^{C} and PrP^{Sc}, particularly an increase in the β-sheet content in PrP^{Sc} [3]. Two prominent models are those of conformational change within a PrP^{C}/PrP^{Sc} heterodimer [4] and of seeded polymerisation, in which a PrP^{Sc} polymer grows from a population of individual PrP molecules that fluctuate between PrP^{C} and PrP^{Sc} states [5]. The two models can be combined if PrP^{C} is postulated to bind to a PrP^{Sc} polymer prior to conformational conversion [6]. The relative infectivity of TSEs compared with other amyloidoses [1] would be consistent with the recruitment of an evolved interaction. For example, a PrP^{C}/PrP^{Sc} heterodimer could exchange monomers between PrP^{C} and PrP^{Sc} homodimers, with the PrP^{Sc} homodimer cross-linked to a polymer through a separate interaction [7].

Solution structures have been reported for a fragment 121–231 and full length 23–231 recombinant mouse PrP (MoPrP) [8,9] and for a larger fragment 90–231 and full length 29–231 recombinant Syrian hamster PrP (SHaPrP) [10,11]. The fold of PrP(121–231) is consistent between these studies, presumably reflecting the core PrP^{C} structure. The amino-terminal region, containing the peptide repeat that binds copper in vitro [12] and in vivo [13], is mobile in these reports. This region is not required for PrP^{Sc} propagation [14]. The solution structures provide a starting point for modelling the PrP^{C}/PrP^{Sc} conversion that is likely to feature in many forms of PrP-related neurodegenerative disease, although disease-causing mutations can also be associated with an altered PrP translocation in the endoplasmic reticulum [15].

This article considers predictions of pH-dependence for MoPrP(121–231) and for HuPrP(90–231) modelled from SHaPrP(90–231), alongside unfolding characterisations that have identified a β-rich intermediate in the presence of denaturant at an acidic pH [16,17]. The predicted pH-dependence supplies hypotheses that can be tested by mutagenesis. Calculations of PrP complementarity with a negatively-charged membrane surface are added in considering the potential involvement of PrP-membrane and PrP-PrP interactions in the prion pathogenesis, including discussion of the protective effects of certain basic polymorphisms in terms of possible membrane-induced stabilisation of PrP^{C} rather than interactions with a protein X [18].

2. Materials and methods

2.1. PrP structures

Solution structures were obtained from the Protein Data Bank, 1ag2 for MoPrP(121–231) [8,19] and 2prp for SHaPrP(90–231) [10]. The 1ag2 set contains a single refined conformer. A model for HuPrP(90–231) was constructed from conformer seven of the unrefined SHaPrP(90–231) coordinates, with 18 amino acid changes (eight involving ionisable groups), with the program QUANTA (Molecular Simulations). Additional sidechain torsions were applied to alleviate close contacts for ionisable residues. The HuPrP(90–231) model maintains the 3D framework of the SHaPrP(90–231) structure.

2.2. Calculations of the pH-dependence

Charge-charge interactions were calculated with the Debye-Hückel (DH) method, using a uniform relative dielectric of 80 and a ionic strength at 0.15 M. This model is more robust in overall comparisons to experimental pK_as than are current implementations of more detailed methods that incorporate a lower dielectric response, since most ionisable group interactions are dominated by solvent-like dielectric properties [20]. Calculations included R, K, H, D and E residues, as well as the N- and C-terminal groups of the HuPrP(90–231) model. The two cysteines (179 and 214 in human PrP) are disulfide-bonded and tyrosine ionisation has been omitted in this study which concentrates on neutral and acidic pH. Polar hydrogen atoms were retained and non-polar hydrogen atoms removed from the coordinates and ionisable group and partial charges [21] assigned. A statistical treatment of interacting groups was used for pK_a calculations [22]. The pH-dependence of ΔG_{NU}, the free energy difference between native and unfolded states, was calculated with DH application to the native PrP structures and to a simple model for ionisable group interactions in the unfolded form. This model gives a significantly improved match

*Corresponding author. Fax: (44) (118) 926 7917.
E-mail: james.warwicker@bbsrc.ac.uk

[1] Current address: Institute of Biomedical and Life Sciences, University of Glasgow, Glasgow G12 8QQ, UK.
Fax: (44) (141) 330 6545. E-mail: j.warwicker@bio.gla.ac.uk

PII: S0014-5793(99)00428-7

to the experiment, based largely on nearest neighbour ionisable residue interactions in the unfolded state [20].

2.3. Calculation of PrP-membrane charge interactions

A program was written to assess the complementarity between PrP charges and a negatively-charged surface, such as a phospholipid membrane. The planar surface contacts the protein at tangents to radii that describe a sphere. In each orientation, the interaction was summed over groups carrying a net charge. Each charge, at distance z from the membrane, interacts with a potential $\Phi = \Phi_0 \exp(-\kappa z)$, with $\Phi_0 = \sigma/(\varepsilon\varepsilon_0\kappa)$, where κ is the Debye-Hückel factor (at 0.15 M ionic strength), ε_0 is the zero permittivity, ε is the relative dielectric (80) and σ is the surface charge density (77 Å^2 for each negative charge). Interactions were contoured on a spherical shell for display in the program QUANTA running on a Silicon Graphics workstation. These calculations are empirical, with a smeared membrane charge and without optimisation of protein sidechain-membrane interactions. A similar analysis for non-polar interactions is more difficult since solvent accessible area is highly dependent on a conformational detail that is not well-defined in this model.

3. Results and discussion

3.1. Calculations of the pH-dependence

Fig. 1A shows the calculated acid pH-dependence of ΔG_{NU} for HuPrP(90–231) that has been modelled from SHa(90–231). For this fragment, $\Delta G_{NU} = -19$ kJ/mol at a neutral pH (measured in guanidinium hydrochloride, GuHCl), with a native-like secondary structure down to pH 2.6 in the absence of denaturant, but an only marginal stability to GuHCl at pHs 2.6, 3.6 and 4.0 [16]. The pH-dependence calculations are consistent with these data, with a marginal stability at a low pH, supporting their use in predictive modelling.

The non-polar surface area is exposed in HuPrP(90–231) in a process with a pK_a of about 5.1 that does not involve global loss of the native-like secondary structure [16]. Since 90–120 is relatively mobile in the SHaPrP(90–231) solution structure, it is likely that the native secondary structure is associated with the 121–231 folding core and that the non-polar surface exposure relates to a change in the average properties of the 90–120 segment. Such a change would be consistent with the reported contrast between the sensitivity of SHaPrP(90–231) to solution conditions around pH 5.2 and the lower pH of 4.5 for the MoPrP(121–231) structure [10]. Candidate ionisable groups for mild acidic pH transitions present in PrP(90–231), but apparently absent in PrP(121–231), are clear. Both HuPrP and SHaPrP have two histidine and four lysine residues within 90–120. Only H-96 and H-111 have calculated pK_as between 5 and 6 in HuPrP(90–231) and sequence considerations alone suggest that the basic charge concentration could push these histidine pK_as towards a mild acidic pH. If the highly-conserved segment within 90–128 mediates functional PrP^C-PrP^C interactions, then, such histidine pK_as could determine the oligomeric status at a mild acidic pH [6], perhaps linking to titration of copper-octarepeat binding at about pH 6 [23] if an acidic intracellular (endosomal) compartment is involved. It is therefore suggested that mutation of H-96 and H-111 could probe the pH-dependence both in vitro and in vivo.

The β-rich intermediate that appears at a mild acidic pH in the presence of denaturant involves a significant structural change in the 121–231 folding core [17]. For MoPrP(124–226), the resolved polypeptide in the MoPrP(121–231) structure, Fig. 1B gives calculated pH-dependences for the G_N and G_U components of ΔG_{NU}. These are separated by the measured ΔG_{NU} (urea denaturation) of −28.6 kJ/mol at a neutral pH [17]. Again, the calculations are consistent with the measured PrP fragment stability at acidic pH. The β-rich intermediate, which complicates the comparison of theory and experiment for ΔG_{NU} at an acidic pH, is viewed as a potential link to PrP^{Sc}. Fig. 1B shows schematically a plausible overall relationship between native, unfolded and intermediate state stabilities. Intermediate (I) appears at pH 5 in the presence of denaturant, indicating a stability between N and U, whilst increasing I as the pH is lowered to 4 in the absence of denaturant [17], suggesting a hypothetical N/I intercept that is drawn at pH 3.5 (this intercept occurs at a lower pH for HuPrP(90–231), which has a native-like secondary structure at pH 2.6 [16]). The simple observation is that experimental characterisations of a β-rich intermediate are consistent with a scheme in which the acid pH-dependence of the stability is significantly less for I than for N and that we can therefore use the predicted G_N to look at factors that may contribute to I formation at an acidic pH.

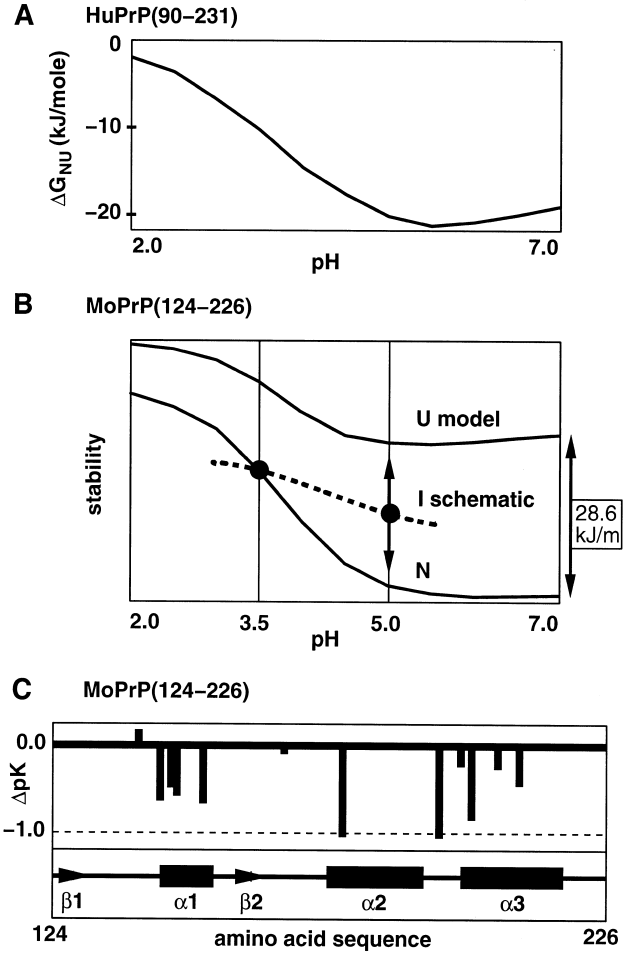

Fig. 1. Calculated acid pH-dependence for PrP fragments. A: The predicted ΔG_{NU} for modelled HuPrP(90–231) is fixed at the measured neutral pH value, $\Delta G_{NU} = -19$ kJ/mol [16]. B: The predicted pH-dependence of MoPrP(124–226) G_N and G_U are shown with an arbitrary overall origin and separated by −28.6 kJ/mol at pH 7 [17]. The schematic I plot shows a possible β-rich intermediate pH-dependence in the indicated pH range (see Section 3). C: Calculated D, E and H ΔpK_as in native MoPrP(124–226) are displayed in the context of the secondary structure [19].

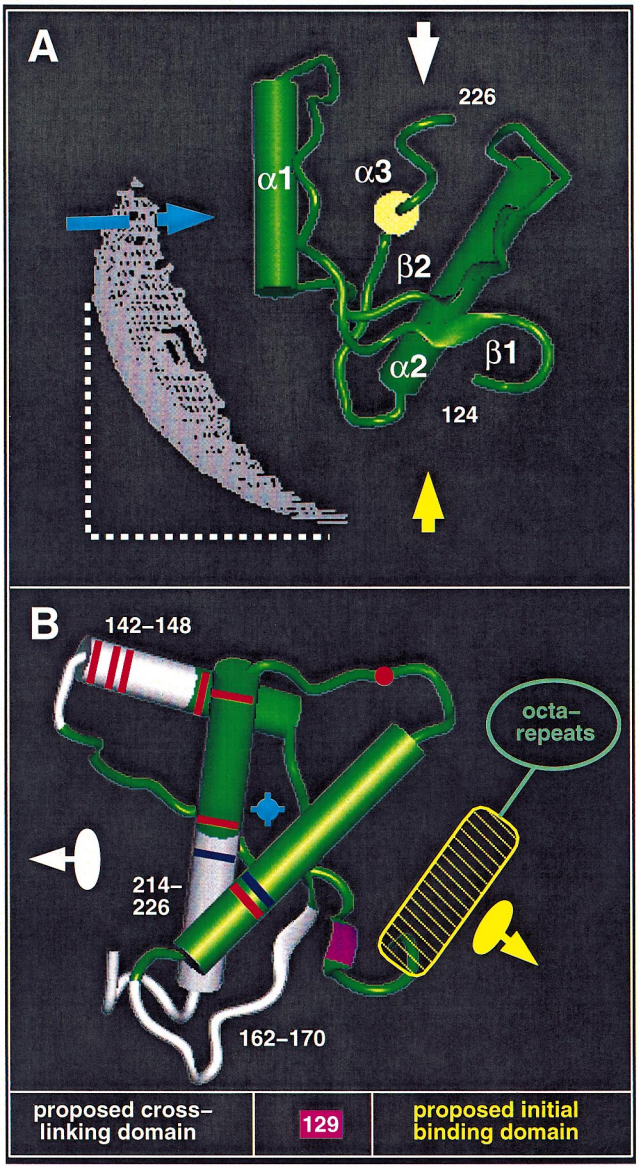

Fig. 2. Modelling interaction domains in PrP. A: Calculated charge complementarity of MoPrP(124–226) [19] with a negatively-charged membrane. The white contour shows favourable interactions at a level of −20 kJ/mol, with the membrane lying at a tangent to each shell radius. The blue arrow denotes a potential membrane binding face and yellow and white arrows denote potential PrP-PrP interaction domains shown also in B. The view is along helix 3, the cross-section of which appears in yellow. B: A view onto the top of a putative PrP-membrane complex shows in white the three segments of a PrP^{Sc}-specific epitope [29], whilst the yellow schematic 90–123 segment adjoins the MoPrP(124–226) fragment N-t and occupies a similar region to the relatively labile equivalent part in the SHaPrP(90–231) structure [10]. Blue stripes show the disulfide-bonded residues C-179 and C-214 and purple marks the human polymorphic site 129. Red markers give the eight residues of Fig. 1C that have $\Delta pK_a < -0.3$: D-144, E-146, D-147, E-152, D-178, E-196, D-202 and E-211.

The predicted acid pH-dependence of G_N (and G_U) arises largely from diminishing favourable interactions as D/E residues bind protons at pH < 5. Fig. 1C shows the calculated ΔpK_as of D, E and H residues within native MoPrP(124–226). Significant negative ΔpK_as (denoting N stabilisation at a neutral pH), are located in α1 and the α2-α3 segment. The large ΔpK_a (−1.06) at the start of α2 relates to the pathogenic mutation D178N. The calculated ΔpK_a of E200 is only −0.23, since this sidechain extends into solvent rather than forming a helix N-cap in the solution structure [19], with the E200K charge reversal predicted to give just one half of the D178N effect. Computed destabilisation of E200K relative to wild-type by about 3 kJ/mole is in good agreement with a recently reported experimental determination of 4 kJ/mole [24]. It appears generally that some pathogenic PrP mutations may be linked predominantly to native state destabilisation, whilst others will require a more detailed understanding of the conversion process and PrP^{Sc} structure [25]. The extent of pH-dependence in N, U and I could be assessed from measurements of proton titration over accessible acidic pH ranges for wild-type and mutant PrPs.

Calculations of energy differences, for example relating to pathogenic mutations, are hampered by a lack of structural information for PrP^{Sc}. In addition, the β-rich intermediates characterised in vitro [16,17] do not form β-cross-links between molecules [3], suggesting the involvement of other components in vivo. However, these intermediates are of significant interest and the current modelling highlights the potential role and relative effects of acidic residues in the folding core. The calculations are inconsistent with the substantial increase in the MoPrP(121–231) stability from pH 7 to pH 4.5 that would be obtained from comparison of $\Delta G_{NU} = -28.6$ kJ/mol to the sum of ΔG_{NI} (−31.1 kJ/mol) and ΔG_{IU} (−22.4 kJ/mol) at pH 4.5 [17]. Assumptions involved in ΔG extrapolation to a zero denaturant concentration, complicated by the three-state system, may contribute to this discrepancy.

3.2. Calculation of PrP-membrane charge complementarity

Fig. 2A shows modelled MoPrP(124–226) interactions with an anionic membrane surface at neutral pH and with a net protein charge of −0.5e. A positively-charged PrP face and its potential for membrane interactions has been noted previously [8]. The current calculation shows a clearly-defined contiguous set of favourable binding orientations. The blue arrow denotes membrane binding to the positively-charged face that includes helix α1. At right angles, the yellow arrow points into the fragment N-t. Considerations of polarity, conservation and species barriers gave rise to the suggestion that PrP could interact with the membrane surface in either of these orientations [7]. This suggestion is now refined with the reported specificity of inhibition of the in vitro conversion reaction with respect to peptides within 106–141 and residues G119 and A120 in particular [26]. Such a specificity implies a protein-peptide interaction so that a single overall PrP-membrane orientation is now favoured, with the region adjacent to the N-t at 124 (yellow arrow) mediating protein-protein interactions and putative membrane binding to the α1-containing face (blue arrow). The right angle indicates that symmetric PrP-PrP interactions could occur across the membrane surface. Whilst PrP^{C} is readily released from a membrane by cleavage of its glycosylphospatidylinositol anchor [27], the calculations suggest that PrP-membrane charge interactions could influence the PrP orientation through summation in an aggregate.

3.3. Modelling interaction domains within PrP(90–231)

Predictions of the pH-dependence and PrP-membrane interactions are considered in the context of data relating to PrP^{C}/

PrP^{Sc} conformational changes [28,29] and protein X binding [18]. Fig. 2B looks onto a potential PrP-membrane complex (into the blue arrow of Fig. 2A). Proposed membrane binding to the α1-containing face and PrP-PrP binding involving the conserved non-polar segment gives two interaction domains. The specificity of interactions involving the latter region [26] may reflect PrP^{C}/PrP^{Sc} interactions that are recruited from PrP^{C}/PrP^{C} [6]. This segment is not necessary for formation of the in vitro β-rich intermediate [17] and it is labelled the initial binding domain.

The three segments of a PrP^{Sc}-specific epitope, that is common in BSE, scrapie and CJD, presumably become neighbours in PrP^{Sc} [29]. This could occur with a dimeric or approximately dimeric interaction on the membrane surface, with symmetry-related 214–226/162–170 adjacent to 142–148, suggesting that this part of PrP could form a third interaction domain (Fig. 2B). Taken together, these three domains could mediate membrane-templated PrP polymer formation. Siting of species barrier residues in the highly-conserved segment and at 139 (human PrP numbering) [30] is consistent with dimeric interactions across both proposed PrP-PrP interaction domains. Of the eight D and E residues with predicted $\Delta pK_a s < -0.3$ in native MoPrP(124–226), four are located around the 142–148 segment and two are adjacent to the 214–226 and 162–170 segments (Fig. 2B). Stabilisation of D/E residues in α1 arises from interactions with the basic residues that determine the membrane charge complementarity. These D/E locations suggest that the PrP^{Sc}-specific epitope may be associated with a conformational change during the in vitro N/I transition and possibly the PrP^{C}/PrP^{Sc} conversion. Proposed cross-linking, mediated by this domain, may therefore be concomitant with a conformational change.

Involvement of the 214–226 segment in conversion would not necessarily preclude antibody accessibility to 225–231 in PrP^{Sc} and PrP^{C} [28]. Equally, an epitope within 95–104 that is exposed in PrP^{C} and largely cryptic in PrP^{Sc} [28] does not preclude PrP^{C}/PrP^{Sc} differences in other regions. In this model, different antibody reactivities with 95–104 would relate to dimerisation across the conserved non-polar region that is transient in PrP^{C}, but longer lived in PrP^{Sc} due to the addition of polymer cross-linking interactions associated with α/β-transition in more C-t regions.

Basic polymorphisms at sites (human PrP numbering) 168, 172, 215 and 219 that protect against conversion are thought to form part of an epitope for protein X binding to PrP, rendering it unavailable for prion propagation [18]. Calculations with the current model show that basic sidechains are predicted to have varying effects on the PrP^{C} stability and PrP^{C} stability in the presence of a negatively-charged membrane. Whilst Q168R is calculated to give intrinsic PrP^{C} stabilisation, basic residues at 215 or 219 could stabilise PrP^{C} through favourable interactions with the membrane. Such modelling therefore suggests an alternative explanation for the protective effects of these basic polymorphisms, particularly since these sites lie within regions of a proposed PrP^{C}/PrP^{Sc} conformational change. Not all basic substitutions would necessarily have a native state stabilising effect. For example, the pathogenic mutation Q217R in humans [2] could destabilise PrP^{C} through loss of a hydrogen bond between the sidechain amide and the mainchain carbonyl of A133 [19].

Biochemical strain-typing [31] is based on measurements of protease resistance and glycoform levels in PrP^{Sc}. These could relate to packing variations within a polymer formed on a membrane (but probed after membrane solubilisation). The human polymorphic residue 129 is sited between proposed interactions domains (Fig. 2B) and could therefore influence packing. Both *N*-linked glycosylation sites are exposed and without steric restriction in the PrP-membrane complex of Fig. 2B. Glycosylation generally stabilises proteins [32]. If glycosylation stabilises PrP^{C} and if the PrP^{C} stability plays a role in pathogenesis, then, in PrP^{Sc} seed formation (as opposed to propagation), it may be that sporadic TSEs would incorporate a lower glycosylation (less stable PrP^{C}) and that those inherited TSEs that derive from PrP^{C} destabilising mutations would tend more towards the available range of glycosylation. Propagation of glycoform levels could relate to packing or size exclusion effects that trace back to the seed. The link between strain-typing by protease resistance and glycoform levels and by a bioassay and lesion profiling is unknown, but presumably entails the interaction of a region-specific cellular property, such as the PrP^{C} production level or rate of PrP^{Sc} clearance [2], with a PrP^{Sc}-specific property. One candidate for this latter property could be simply the effect of the PrP^{Sc} glycoform composition on the amount of PrP^{C} that is accepted for conversion.

3.4. Testing the model

The current model has been developed alongside existing data and can be tested with further measurements. Mutation of (human PrP numbering) H-96 and H-111 within PrP(90–231) would probe any role in the process of non-polar surface area exposure around pH 5.1 that does not involve global loss of the native-like secondary structure [16]. The model predicts that the conserved non-polar segment within 90–120 is crucial to an initial binding step that precedes α to β structure conversion. This hypothesised initial binding could be probed with resolution of the order of binding and conversion, thereby distinguishing this model and those that invoke conversion before, or concomitant with, initial binding.

With respect to characterisation of the β-rich in vitro intermediate, our calculations suggest that removal of a sidechain negative charge at the following locations will destabilise PrP^{C} and potentially enhance the intermediate formation: 196, 178, 202, 152, 144, 147, 146, 211. This listing ranks the predicted destabilisations from about 6 kJ/mole (196, 178) to about 2 kJ/mole (211). It would be of interest to assess whether the β-rich intermediate is less accessible for PrP with *N*-linked glycosylation.

The suggestion that the protective effects of basic sidechains at certain polymorphic sites could relate to PrP^{C} stabilisation in the presence of a membrane could be probed with measurements of recombinant PrP interactions with a negatively-charged surface, particularly the effects of positive charges at 215 and 219. A predicted membrane involvement in the PrP^{Sc} formation could be studied with in vitro conversion efficiencies in the presence and absence of membrane components.

The three modelled interaction domains (Fig. 2) suggest strategies for designing recombinant PrPs with PrP^{Sc}-like properties in the absence of the putative membrane templating and for considering potential inhibitors of PrP^{Sc} formation. Designed destabilisation of the proposed cross-linking (α/β conversion) domain together with stabilisation of the proposed initial dimerisation may increase the susceptibility to

PrP^{Sc} formation. We have suggested that the membrane plays a role in this putative dimerisation in vivo through biasing the orientation and configuration, perhaps aided by the three conserved lysine residues (101, 104, 106) on the N-t side of the non-polar segment. Dimerisation without membrane may therefore be enhanced by the introduction of an adjacent complementary acidic patch on PrP or by a cross-linking strategy that brings together the non-polar segments of two PrP molecules. The model suggests that polyanionic inhibitors [33] could interact with the proposed membrane binding domain and that more effective inhibitors of PrP^{Sc} formation should link such an activity with elements targeted at sequences in the proposed dimerisation and cross-linking domains.

References

[1] Chesebro, B. (1998) Science 279, 42–43.
[2] Prusiner, S.B., Scott, M.R., DeArmond, S.J. and Cohen, F.E. (1998) Cell 93, 337–348.
[3] Pan, K.-M., Baldwin, M., Nguyen, J., Gasset, M., Serban, A., Groth, D., Mehlhorn, I., Huang, Z., Fletterick, R.J., Cohen, F.E. and Prusiner, S.B. (1993) Proc. Natl. Acad. Sci. USA 90, 10962–10966.
[4] Prusiner, S.B. (1991) Science 252, 1515–1522.
[5] Caughey, B., Kocisko, D.A., Raymond, G.J. and Lansbury, P.T. (1995) Chem. Biol. 2, 807–817.
[6] Warwicker, J. and Gane, P.J. (1996) Biochem. Biophys. Res. Commun. 226, 777–782.
[7] Warwicker, J. (1997) Biochem. Biophys. Res. Commun. 238, 185–190.
[8] Riek, R., Hornemann, S., Wider, G., Billeter, M., Glockshuber, R. and Wüthrich, K. (1996) Nature 382, 180–182.
[9] Riek, R., Hornemann, S., Wider, G., Glockshuber, R. and Wüthrich, K. (1997) FEBS Lett. 413, 282–288.
[10] James, T.L., Liu, H., Ulyanov, N.B., Farr-Jones, S., Zhang, H., Donne, D.G., Kaneko, K., Groth, D., Mehlhorn, I., Prusiner, S.B. and Cohen, F.E. (1997) Proc. Natl. Acad. Sci. USA 94, 10086–10091.
[11] Donne, D.G., Viles, J.H., Groth, D., Mehlhorn, I., James, T.L., Cohen, F.E., Prusiner, S.B., Wright, P.E. and Dyson, H.J. (1997) Proc. Natl. Acad. Sci. USA 94, 13452–13457.
[12] Hornshaw, M.P., McDermott, J.R., Candy, J.M. and Lakey, J.H. (1995) Biochem. Biophys. Res. Commun. 214, 993–999.
[13] Brown, D.R., Qin, K., Herms, J.W., Madlung, A., Manson, J., Strome, R., Fraser, P.E., Kruck, T., von Bohlen, A., Schulz-Schaeffer, W., Giese, A., Westaway, D. and Kretzschmar, H. (1997) Nature 390, 684–687.
[14] Fischer, M., Rülicke, T., Raeber, A., Sailer, A., Moser, M., Oesch, B., Brandner, S., Aguzzi, A. and Weissmann, C. (1996) EMBO J. 15, 1255–1264.
[15] Hegde, R.S., Mastrianni, J.A., Scott, M.R., DeFea, K.A., Tremblay, P., Torchia, M., DeArmond, S.J., Prusiner, S.B. and Lingappa, V.R. (1998) Science 279, 827–834.
[16] Swietnicki, W., Petersen, R., Gambetti, P. and Surewicz, W.K. (1997) J. Biol. Chem. 272, 27517–27520.
[17] Hornemann, S. and Glockshuber, R. (1998) Proc. Natl. Acad. Sci. USA 95, 6010–6014.
[18] Kaneko, K., Zulianello, L., Scott, M., Cooper, C.M., Wallace, A.C., James, T.L., Cohen, F.E. and Prusiner, S.B. (1997) Proc. Natl. Acad. Sci. USA 94, 10069–10074.
[19] Billeter, M., Riek, R., Wider, G., Hornemann, S., Glockshuber, R. and Wüthrich, K. (1997) Proc. Natl. Acad. Sci. USA 94, 7281–7285.
[20] Warwicker, J. (1999) Protein Sci. 8, 418–425.
[21] Van Gunsteren, W.F. and Berendsen, H.J.C. (1987) GROMOS Manual, University of Groningen, Groningen, The Netherlands.
[22] Bashford, D. and Karplus, M. (1990) Biochemistry 29, 10219–10225.
[23] Stöckel, J., Safar, J., Wallace, A.C., Cohen, F.E. and Prusiner, S.B. (1998) Biochemistry 37, 7185–7193.
[24] Swietnicki, W., Petersen, R.B., Gambetti, P. and Surewicz, W.K. (1998) J. Biol. Chem. 273, 31048–31052.
[25] Riek, R., Wider, G., Billeter, M., Hornemann, S., Glockshuber, R. and Wüthrich, K. (1998) Proc. Natl. Acad. Sci. USA 95, 11667–11672.
[26] Chabry, J., Caughey, B. and Chesebro, B. (1998) J. Biol. Chem. 273, 13203–13207.
[27] Stahl, N., Borchelt, D.R. and Prusiner, S.B. (1990) Biochemistry 29, 5405–5412.
[28] Peretz, D., Williamson, R.A., Matsunaga, Y., Serban, H., Pinilla, C., Bastidas, R.B., Rozenshteyn, R., James, T.L., Houghten, R.A., Cohen, F.E., Prusiner, S.B. and Burton, D.R. (1997) J. Mol. Biol. 273, 614–622.
[29] Korth, C., Stierli, B., Streit, P., Moser, M., Schaller, O., Fischer, R., Schulz-Schaeffer, W., Kretzschmar, H., Raeber, A., Braun, U., Ehrensperger, F., Hornemann, S., Glockshuber, R., Riek, R., Billeter, M., Wüthrich, K. and Oesch, B. (1997) Nature 390, 74–77.
[30] Priola, S.A. and Chesebro, B. (1995) J. Virol. 69, 7754–7758.
[31] Collinge, J., Sidle, K.C.L., Meads, J., Ironside, J. and Hill, A.F. (1996) Nature 383, 685–690.
[32] Wang, C., Eufemi, M., Turano, C. and Giartosio, A. (1996) Biochemistry 35, 7299–7307.
[33] Demaimay, R., Harper, J., Gordon, H., Weaver, D., Chesebro, B. and Caughey, B. (1998) J. Neurochem. 71, 2534–2541.